On the effect of wind speed on submicron sea salt mass concentrations and source fluxes

Jurgita Ovadnevaite,[1] Darius Ceburnis,[1] Manjula Canagaratna,[2] Harald Berresheim,[1] Jakub Bialek,[1] Giovanni Martucci,[1] Douglas R. Worsnop,[2,3] and Colin O'Dowd[1]

Received 22 December 2011; revised 27 June 2012; accepted 3 July 2012; published 16 August 2012.

[1] A High Resolution Time of Flight Aerosol Mass Spectrometer (HR-ToF-AMS) was evaluated for its ability to quantify submicron sea salt mass concentrations. The evaluation included both laboratory and field studies. Quantification of the sea salt signal in the HR-ToF-AMS was achieved by taking the $^{23}Na^{35}Cl^{+}$ ion as a surrogate for sea salt and then identifying a calibration scaling factor through a comparison with mono-disperse laboratory generated sea salt aerosol. Ambient sea salt concentrations calculated using this method agreed well with those obtained by ion chromatography of filter samples, following a 1:1 regression slope and a correlation coefficient $R = 0.93$. A key advantage of this AMS-based method is that it allows for high time resolution measurements of sea salt (5 min) along with the speciation of other chemical compounds, including primary organics contributing to sea spray. The high-time resolution sea salt measurement capability enabled the quantification of sea salt mass in both increasing and decreasing wind speed regimes up to 26 m s^{-1}. A mass flux source function was also derived and found to have a power law wind speed dependency with an exponent of 3.1 for increasing winds and 2.3 for decreasing winds. Comparison of the mass flux relationship in this study suggests that previous schemes based on the Monahan whitecap–wind speed approach significantly over-estimate the submicron mass flux. Both the whitecap–wind speed component and the differential whitecap–aerosol productivity component of the source flux function contribute toward the over-estimation.

Citation: Ovadnevaite, J., D. Ceburnis, M. Canagaratna, H. Berresheim, J. Bialek, G. Martucci, D. R. Worsnop, and C. O'Dowd (2012), On the effect of wind speed on submicron sea salt mass concentrations and source fluxes, *J. Geophys. Res.*, *117*, D16201, doi:10.1029/2011JD017379.

1. Introduction

[2] Sea spray aerosol is an important component of the aerosol population in the marine environment, and given that 70% of the Earth's surface is covered by oceans, sea spray contributes significantly to the global aerosol budget [*Vignati et al.*, 2010]. In addition, sea spray plays an important role in climate, with both direct [*Mulcahy et al.*, 2008] and indirect radiative effects [*O'Dowd et al.*, 1999]. In order to better understand and quantify these effects, detailed information on the chemical composition, the size distribution and the abundance is required. Until recently, sea spray was generally assumed to be composed predominantly of inorganic sea salt. However, recent findings [*Facchini et al.*, 2008; *O'Dowd et al.*, 2004] revealed a sometimes predominant organic fraction in submicron marine aerosol mass, with organic mass fraction enrichment in the spray reaching up to 80%. These observations prompted the development of a combined organic-inorganic sea spray source function for implementation in climate and chemical transport modeling studies [*Gantt et al.*, 2011; *O'Dowd et al.*, 2008; *Vignati et al.*, 2010]. Model evaluation and verification, however, benefits from long-term ambient measurements and these measurements have historically derived from filter or impactor studies with typical sampling periods of ~1 day for bulk mass, and ~7 days, for size resolved mass distributions in marine air. Such integrated measurements are more likely to miss higher temporal structure in the data signals, and as a result of this, peak concentrations are likely to be missed. An improvement was made by deploying near real time techniques such as Particle Into Liquid Samplers (PILS), which are capable of measuring the main inorganic ions along with soluble organics at a high time resolution [*Sullivan et al.*, 2004; *Weber et al.*, 2003] or Aerosol Mass Spectrometry techniques for the nonrefractory aerosol composition measurements. Indeed, recent deployment of high temporal

[1]School of Physics and Centre for Climate and Air Pollution Studies, Ryan Institute, National University of Ireland Galway, Galway, Ireland.
[2]Aerodyne Research, Inc., Billerica, Massachusetts, USA.
[3]Physics Department, University of Helsinki, Helsinki, Finland.

Corresponding author: J. Ovadnevaite, School of Physics and Centre for Climate and Air Pollution Studies, Ryan Institute, National University of Ireland Galway, University Road, Galway, Ireland. (jurgita.ovadnevaite@nuigalway.ie)

0148-0227/12/2011JD017379

resolution aerosol mass spectrometry to chemically characterize marine organic aerosol has improved our understanding of primary marine organics and has revealed primary marine organic aerosol plumes at mass concentrations far higher than previously reported [*Ovadnevaite et al.*, 2011]. Hitherto, there has been no equivalent measurement, in terms of temporal resolution, for primary sea spray leading to a lack of high resolution information on primary sea salt mass along with associated primary organic mass enrichment factors.

[3] The High Resolution Time of Flight Aerosol Mass Spectrometer (HR-ToF-AMS) is designed to provide high-time resolution measurements of aerosol chemical composition with spectral resolution that allows for distinguishing multiple ions at the same nominal mass to charge ratio (m/z) [*DeCarlo et al.*, 2006]. Typically the AMS is operated at a vaporizer temperature of 600°C, which is optimized for quantitative detection of non-refractory ambient aerosol species such as organics, sulfate, nitrate and ammonium. Since sea salt was expected to be refractory at these temperatures, its quantification with the AMS was assumed to be only possible at higher AMS vaporizer temperatures that were less favorable for quantification of the non-refractory species [*Allan et al.*, 2004]. However, *O'Dowd and Smith* [1993] demonstrated that ambient sea salt starts to evaporate at temperatures just above 600°C and almost fully evaporates at 650°C, suggesting that the standard HR-ToF-AMS operation temperature could be sufficient to detect sea salt.

[4] This study evaluates the suitability of deploying the HR-ToF-AMS to undertake quantitative sea salt measurements at close to standard operating conditions and applies the technique to determine the concentration of sea salt as a function of wind speed.

2. Experimental Setup for Ambient Air Measurements

[5] The study was undertaken at the Mace Head Atmospheric Research Station located on the west coast of Ireland facing the North East Atlantic. Station details are found in *O'Connor et al.* [2008]. All aerosol instruments are located in the shore laboratory about 100 m from the coastline and 5 m above mean sea level. They are connected to the laminar flow community air sampling system, which is constructed from a 100 mm diameter stainless-steel pipe with the main inlet at 10 m above ground level. The performance of this inlet is described in *Kleefeld et al.* [2002].

[6] The HR-ToF-AMS [*DeCarlo et al.*, 2006] was used for chemical composition measurements and was routinely calibrated according to the methods described by *Jimenez et al.* [2003] and *Allan et al.* [2003]. The HR-ToF-AMS was connected to the main community sampling system retaining an iso-kinetic flow. A performance of this set up was tested with 2 scanning mobility particle sizers (SMPSs) and 2 condensation particle counters (CPCs): one of each instrument was sampling from the main inlet directly and the second in front of the HR-ToF-AMS, differences between the measurements were found to be within the instruments uncertainty range (~10%). The HR-ToF-AMS measurements were performed with a time resolution of 5 min and a vaporizer current of 1.12 A (corresponding to a vaporizer temperature of ~650°C). The net overall particle transmission and detection efficiency, expressed as the collection efficiency (CE), is dependent on the particle composition. Therefore, a composition dependent CE [*Middlebrook et al.*, 2012] was applied for the measurement periods discussed in this study. CE ranged from 0.45 to 0.97. The default CE of 0.5 was deemed appropriate for ~40% of the periods of interest and dominated particularly in continental air masses. A CE of ~1 corresponded to ~60% of the measurement period and was observed for both clean marine air masses (due to very acidic aerosol) and continental polluted air masses (due to high nitrate episodes). Since sea salt concentrations were low during non-marine periods the original composition dependent CE algorithm presented in the *Middlebrook et al.* [2012] study was used without including the sea salt. The effect of sea salt on aerosol CE was accounted for with a calibration factor, which comprised both the CE and relative ionization efficiency (RIE) of sea salt (see Section 3 for more details).

[7] PM2.5 (particles, or particulate matter less than 2.5 μm in size where 2.5 μm correspond to the 50% collection efficiency size) aerosol samples were taken routinely every other day using an RP 2025 Dichotomous Sampler. The Sampler was installed at the same height as the community sampling duct. The filters from the dichotomous sampler were analyzed using standard Ion Chromatography (IC) methods. Aerosol size distributions were measured using an SMPS. The SMPS system comprised of a differential mobility analyzer (DMA, TSI model 3071), a condensation particle counter (TSI model 3010), and an aerosol neutralizer (TSI 3077). For the sizing purpose, particles were dried below 20% relative humidity. Hygroscopic properties of aerosol were measured using a Hygroscopic Tandem Differential Mobility Analyzer (HT-DMA), as described in *Rader and McMurry* [1986] and followed the European Supersite for Atmospheric Aerosol Research (EUSAAR) network standard configuration and deployment as summarized by *Nilsson et al.* [2009]. An aerosol particle growth factor (GF) at 90% relative humidity (RH), defined as the ratio of the particle diameter at RH = 90% to that at RH = 20%, was determined for dry size particles of 35, 50, 75, 110 and 165 nm.

[8] The wind speed and direction was measured on the 10 m tower by a Vector Instruments wind monitor (model W200P/A100L). The coastal measurements have been extensively compared with the offshore wind data revealing a very good agreement [*Gantt et al.*, 2011].

3. Experimental Setup for Laboratory and Sea Salt Calibration

[9] The HR-ToF-AMS was calibrated using sea salt aerosol generated from artificial seawater using SIGMA sea salt dissolved in deionized water. The solution was nebulized with a TSI atomizer (model 3076), and a DMA configured to generate a 300 nm monodisperse particle size distribution flow from the nebulized polydisperse flow, fed directly into the AMS inlet. Relative humidity in the sample line was maintained at about 65%.

[10] The high resolution mass spectrum was measured and analyzed using the standard high resolution AMS data analysis tool (PIKA v1.10h) [*DeCarlo et al.*, 2006]. 36 high resolution ions contributed to the sea salt fragmentation pattern, but only 7 ions had a significant influence on the

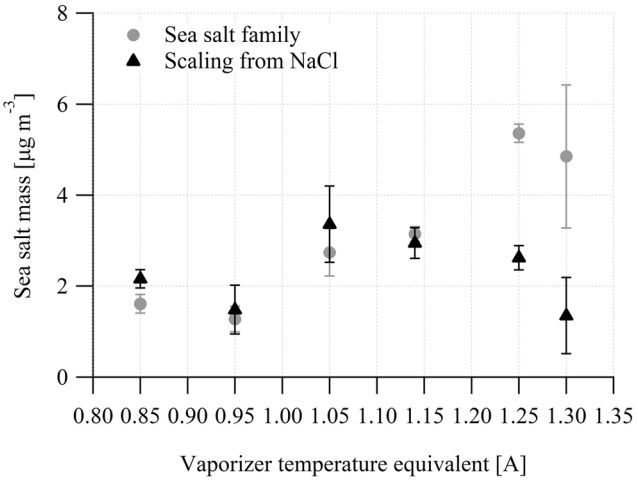

Figure 1. Sea salt detection dependence on the vaporizer temperature obtained for the nebulized artificial seawater. In this graph the temperature is presented as a vaporizer current in order to avoid discrepancies between the real heater temperature and one measured by a thermocouple. Error bars represent standard deviations.

derived aerosol mass, namely $^{23}Na^+$, $^{35}Cl^+$, $H^{35}Cl^+$, $^{23}Na^{35}Cl^+$ and isotopes $^{37}Cl^+$, $H^{37}Cl^+$, $^{23}Na^{37}Cl^+$. Two approaches were chosen to obtain the sea salt mass from the AMS measurements: approach (1) centered on adding up all sea salt ions to obtain a new high resolution sea salt "family", or ensemble, of ions using the data analysis tool and approach (2) centered on using only the $^{23}Na^{35}Cl^+$ ion fragment as the signature of sea salt. Inter-comparisons between these two different approaches to derive AMS sea salt mass with the known sea salt mass concentrations in the laboratory-generated calibration particles were used to derive the scaling factors needed to obtain the quantitative AMS-derived sea salt concentrations. For the first approach, a scaling factor of 2.5 was found to be appropriate for this calibration. The scaling factor for the second approach was much larger, at 51, as only one ion was scaled. The scaling factors derived in these calibrations reflect a combined AMS detection efficiency for sea salt, which encapsulates the AMS collection efficiency and the relative ionization efficiency.

[11] Further investigation into the selected approaches revealed a high Na^+ ion sensitivity to the instrument tuning. A significant proportion of sodium can become ionized thermally rather than by electron ionization. This "surface ionization" is undesirable because it produces positive ions in very large numbers and does not easily yield quantitative data [*Allan et al.*, 2004]. However, by tuning the instrument's heater bias voltage (that is increasing it by 0.1–0.2 V above the normally used maximum value, until the area under the m/z 23 signal rapidly drops, but maintaining optimal signatures for other m/z signals) it is possible to prevent the thermally ionized ions from reaching the detector. Nevertheless, considering that Na^+ has a significant contribution to the sea salt family, the surface ionization could affect a total sea salt quantification if the instrument tuning is not adjusted for the sea salt measurements.

[12] HR-ToF-AMS mass concentrations were obtained by subtracting the general background mass spectrum (i.e., spectrum from aerosol-free carrier gas flow) from the total measured spectra (i.e., from the combined aerosol and gas flow). Although the majority of the gas was removed by differential pumping, providing vacuum down to 10^{-8} Torr, the carrier gas and a slow vaporization from the heater had to be accounted for. Thus, the aerosol beam was alternatively modulated every ~3 s to allow the measurement of both the combined carrier gas and particle mass spectra and the carrier gas-only mass spectra [*DeCarlo et al.*, 2006]. Slowly evaporating compounds lead to a high background mass spectra [*Salcedo et al.*, 2010], which can, depending on the particular species, be comparable to, or even higher than, the measurement signal, resulting in a low signal-to-noise ratio. In these studies, the sodium ion had a high background signal, even exceeding the measurement-signal up to a factor of 10, concomitant with a large delay time. The sodium background signal evaporated completely only 12 h after aerosol flow termination, while Cl^+ and HCl^+ had shorter, but still significant, evaporation times of ~2 h. The slow time-scale for evaporation of the Cl^+, HCl^+ and Na^+ ion signals suggests that these ions are most likely produced by the slow decomposition process associated with the oven surface. In contrast, the $^{23}Na^{35}Cl^+$ background signal was ~10 times lower than the measurement signal, and the evaporation delay time was less than 5 min (i.e., less than the selected averaging time-base of the instrument), indicating the efficient vaporization from the heater.

[13] The test of the instrument's sea salt detection efficiency dependence on vaporizer temperature revealed that the exact fragmentation pattern could be slightly dependent on the heater temperature. For this study, the temperature is presented as a vaporizer current in order to avoid discrepancies between the real heater temperature and one measured by a thermocouple. The vaporizer currents used ranged from 0.85 A (~500°C) to 1.3 A (~800°C). The temperature effect on $^{23}Na^{35}Cl^+$ ion was different from what was anticipated: specifically, a high vaporizer current of 1.3 A negatively affected $^{23}Na^{35}Cl^+$ ion detection, as the signal intensity decreased (Figure 1). This could be explained by two processes: (1) an increase in the fragmentation of $NaCl^+$ ions due to the higher heater temperature, resulting in lower ion concentration and (2) an increase in an ion thermal velocity, which would result in a shorter time that ions spend in the detection region compared to the cooler temperatures associated with lower currents, thus, a decrease in detection [*Allan et al.*, 2004]. In contrast, sodium ion intensity increased with increasing temperature, indicating that higher fragmentation of $NaCl^+$ ion and, partially, surface ionization [*Allan et al.*, 2004] led to a higher Na^+ concentration (Figure 1).

[14] The dependence of AMS sea salt detection efficiency on particle phase (or water content) was evaluated by sampling the highest purity sea salt as possible since even the smallest amount of organic matter internally mixed with sea salt may potentially affect particle behavior under different relative humidities. Sea salt dissolved in deionized water was again nebulized, but in this experiment, the resulting aerosol flow was filtered to select only particles with a GF = 2.2 (i.e., the GF of pure sea salt particles). A nafion drier (Perma Pure PD-200T) was then introduced between the HTDMA output and the HR-ToF-AMS inlet in order to regulate RH while concurrently measuring relative humidity of the flow and sea salt concentration at the same constant

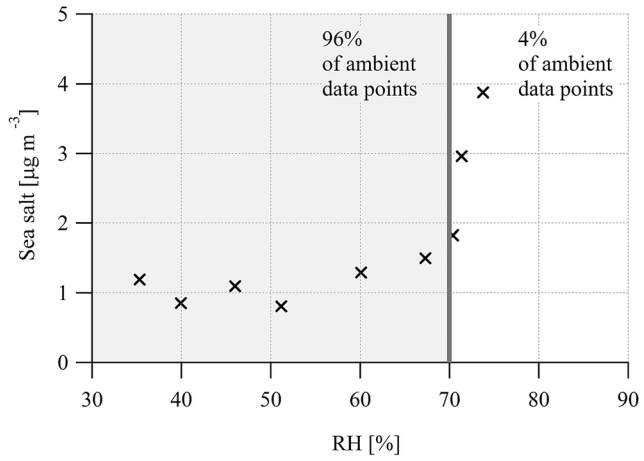

Figure 2. Sea salt detection dependence on the aerosol flow relative humidity obtained for the nebulized artificial seawater. For the comparison, grey zone represents 96% of relative humidity variations in the inlet during ambient measurements.

aerosol supply (in terms of size and number). This experiment revealed that the HR-ToF-AMS quantification depends on the particle phase for RH higher than 70% (Figure 2). The effect of humidity on AMS quantification of sea salt is similar to that previously reported for laboratory $(NH_4)_2SO_4$ particles [*Middlebrook et al.*, 2012]. Previous studies [*Matthew et al.*, 2008; *Middlebrook et al.*, 2012] have shown that the AMS collection efficiency (CE) is dependent on particle phase such that dry particles bounce off the AMS vaporizer while wet particles are collected with unit efficiency. The phase dependent CE of $(NH_4)_2SO_4$, for example, changes sharply from 0.35 at RH < 80% to a CE of 1 at RH > 80%. If we assume the similar behavior for sea salt, the CE of sea salt is likely 1 at >75% RH, and 0.25 at RH < 70% (Figure 2). Accordingly, the sea salt relative ionization efficiency (RIE) can be determined from the scaling factor, which combines the CE (the net overall particle transmission and detection efficiency) and the RIE (the relative ionization efficiency of the species in interest relative to nitrate [*Alfarra et al.*, 2004]) and is equal to (1/CE)*(1/RIE). Considering that CE = 0.25 at RH < 70%, RIE should be ~1.6. Whereas, $NaCl^+$ RIE, could be determined using the $NaCl^+$ fraction in the total sea salt family (~4%), which would result in RIE ~ 2. Typically, the AMS ionization efficiency (IE) reflects vaporization, ionization, and detection efficiencies. However, vaporization and detection is similar across the *m/z* range, thus different RIE classes for inorganic and organic compounds arise from the differences in ionization. Yet these assumptions might not be applicable for the sea salt aerosol, as each of the sea salt ions could be affected to different extents by the vaporization and ionization and these effects can even offset each other. Taking all this into account, RIE numbers presented above should be taken more as guidance, but not the strict values. Moreover, calibration factors may be valid only for this particular instrument (with its particular tuning), thus, every instrument should be calibrated individually in order to derive its own sea salt quantification, or conversion, factor.

[15] It should also be noted that the HR-ToF-AMS measurements at Mace Head are always accompanied by RH measurements within the inlet, immediately up stream of the instrument, and analysis of these data show that 96% of the aerosol entering the AMS were sampled at RH < 70%, suggesting that the Mace Head measurements of AMS-derived sea salt mass are, to a larger degree, free from humidity-driven artifacts.

[16] The above mentioned laboratory tests suggest that second approach of scaling sea salt concentration using the single $^{23}Na^{35}Cl^+$ ion is more robust than the sea salt family approach. Moreover, exploring ambient origins of separate ions included in the possible sea salt ion family indicated that Na^+ and $NaCl^+$ seen by the HR-ToF-AMS come only from sea salt, while Cl^+ and HCl^+ also had significant sources in pollution aerosol as well as marine sources. This is consistent with previous studies [*Chang and Allen*, 2006; *Salcedo et al.*, 2006], which reported that anthropogenic emissions of molecular chlorine during daylight hours readily photolyze and that the resulting atomic chlorine rapidly abstracts hydrogen from hydrocarbons, producing HCl, which in turn reacts with ammonia (NH_3), ultimately producing NH_4Cl. The latter can accumulate in fine particles and be fragmented in the HR-ToF-AMS as Cl^+ ion. Although the contribution from Cl^+ would be lower than that from HCl^+, it would still have an effect in polluted air masses. These implications pointed to an unavoidable need of assigning Cl^+ proportions arising from different sources to some ions without any other source than sea salt. Consequently, the best candidate seemed to be the $NaCl^+$ ion, having a single sea salt origin as well as the largest signal-to-noise ratio. Therefore, constraining the majority of the sea salt ions from the $NaCl^+$ ion would not have any advantage over the second method. Moreover, the latter is much easier to apply and gives consistent measurements. It should be noted; however, that in a marine air influenced by pollution, sea salt can undergo significant processing in terms of Cl displacement by nitric or sulfuric acid, then the sea salt mass derived using the aforementioned approach would not include the processed sea salt component. An extension of the approach could be developed, in principle, to quantify this processed component of sea salt; however, given that we only focus here on pristine marine air masses in N.E. Atlantic air, such an extension is beyond the scope of this work.

4. Comparison of Online and Off-Line Sea Salt Concentrations

[17] Sea salt concentrations derived from the HR-ToF-AMS were compared with concentrations derived from the off-line filter analysis using standard ion chromatography methods. But because the HR-ToF-AMS measures PM1 particles (particles of 1 μm or less in size, where 1 μm corresponds to the 50% sampling efficiency cut-off size) and the routine filter measurements at Mace Head are performed on the PM2.5 particles, differences between absolute measured concentrations were expected, and indeed, found. Moreover, long-term observations at Mace Head indicated a varying ratio between PM1 and PM2.5 mass depending on the season, or more specifically, the enrichment of organics in sea spray. The PM1/PM2.5 percentage ratio ranges from 10 to 25% [*Cavalli et al.*, 2004]. Therefore, different scaling

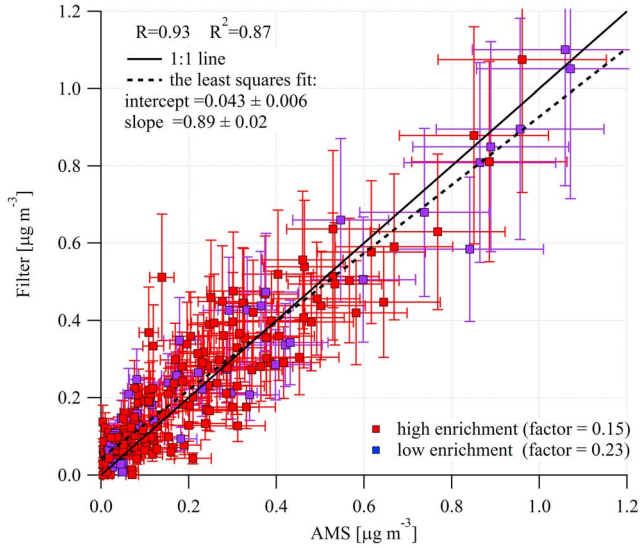

Figure 3. The comparison between the HR-ToF AMS and Ion chromatography sea salt measurements. Colors represent different factors applied for the periods of low and high organic enrichment, when deriving PM1 sea salt concentration from PM2.5 filter measurements. Error bars represent the IC and HR-ToF AMS measurement uncertainties.

factors were applied for the periods of low and high organic enrichment, 0.23 and 0.15, respectively, when deriving PM1 sea salt concentration from the PM2.5 filter measurements. Scaling uncertainties were on the order of 25% and propagated into the total IC measurement uncertainties resulting ~32% overall uncertainty. A comparison between the AMS sea salt measurements, derived from $NaCl^+$ ion, and the PM1 filter sea salt concentration derived from the PM2.5 measurements is presented in Figure 3. The overall HR-ToF-AMS sea salt measurement uncertainty was found to be ~20% and encapsulated the following uncertainties: IE determination uncertainty (~10%); flow uncertainty (~0.5%); lens transmission together with NaCl evaporation from the heater uncertainty (~15%); and scaling uncertainty (~5%). The first two uncertainties were documented in the study of *Bahreini et al.* [2009] and are common for all species measured by the AMS, while the lens transmission, evaporation and scaling uncertainties were evaluated from the sea salt laboratory experiments presented in this study.

[18] Good agreement between the off-line chemical analysis and the AMS sea salt measurements in the field samples supported the results from the laboratory calibrations. The majority (>70%) of the inter-comparison data-points agreed within 20% and the correlation coefficient, R, was equal to 0.93 and R^2 was 0.87. The scatter in the comparison may have arisen from both the AMS collection efficiency and the PM1 scaling factor selected as a function of season. In addition, ion chromatography results also depend on the signal strength and a low signal-to-noise ratio could lead to an overestimation of sea salt mass under low-concentrations conditions [*Elbergali and Brereton*, 1994].

[19] On the other hand, the scaling factors derived in the laboratory calibrations would depend on the lens transmission of the particular instrument as there is some variation between specific aerodynamic lenses in different instruments [*Bahreini et al.*, 2008; *Liu et al.*, 2007; *Zhang et al.*, 2004].

[20] The expected isotope ratio between $^{23}Na^{35}Cl$ and $^{23}Na^{37}Cl$ is equal to 3.13 [*de Laeter et al.*, 2003]. This ratio was, indeed, maintained in the AMS measurements for the comparison period presented above, providing further confidence in the correct sea salt detection.

5. Sea Salt Mass Dependency on Wind Speed

[21] Two cases of elevated-concentration sea salt plumes over North East Atlantic waters are presented in Figure 4, one occurring on the 8th November 2010 and the other on the 11th November 2010. The plumes were detected as the wind direction backed northerly into the clean sector at Mace Head (between 190°–300°) and the wind speed increased to a peak value of 20 m s^{-1} during the first plume and 26 m s^{-1} during the second plume.

[22] Sea salt plumes registered by the AMS coincided with an increase in aerosol hygroscopicity from a typical sulfate GF of 1.6 to a GF of 2.2, which is characteristic of pure sea salt particles. As the measurements were undertaken during the low biological activity period, all other chemical compounds approached very low background "winter" concentrations (e.g., sulfate mass <190 ng m^{-3}; organic mass <60 ng m^{-3}; black carbon mass <10 ng m^{-3}; nitrate mass <17 ng m^{-3} and ammonium mass below the detection limit of 38 ng m^{-3}).

[23] The AMS-derived sea salt mass increased and decreased with wind speed as expected. Although the maximum 5-min mass concentration exceeded 4.5 μg m^{-3}, in the first plume, the running mean peaked at about 2.2 μg m^{-3} while the running mean in the second plume peaked at about 2.4 μg m^{-3}. Both plumes lasted ~30 h. The routine 24 h filter samples missed the plumes due to the sampling strategy employed at Mace Head (i.e., generally every second 24-h period); however, the off-line measurements still would not have captured the fine structure of the sea salt plumes, or the peak concentrations observed by the online AMS if they were run every 24 h period. The two off-line filter samples overlapped with the start and the end of the plume and are in close agreement with the 24 h AMS sea salt averages (Figure 4, bottom). The sea salt plume structure and peak concentrations are quite similar to the structure and concentrations found in the primary organic sea spray plumes observed during periods of high biological activity [*Ovadnevaite et al.*, 2011].

[24] The high time-resolution measurements of sea salt mass enabled the quantification of sea salt mass as a function of increasing and decreasing wind speed as illustrated in Figure 5. Only the second sea salt plume was selected for further analysis due to its greater range of wind speed (i.e., up to 26 m s^{-1}); a higher degree of symmetry in the increasing and decreasing wind speed slopes; and a more stable clean-sector wind direction. Furthermore, this period was practically cloud and precipitation free with only sparse small, fair weather, cumulus cells with intermittent low levels of drizzle.

[25] At the lowest wind speed encountered (i.e., <4 m s^{-1}) both relationships (for increasing and decreasing wind speed) converge on a background submicron sea salt mass concentration of 0.09 μg m^{-3}, and as wind speed increases, they follow a power law mass-concentration versus 10-m wind

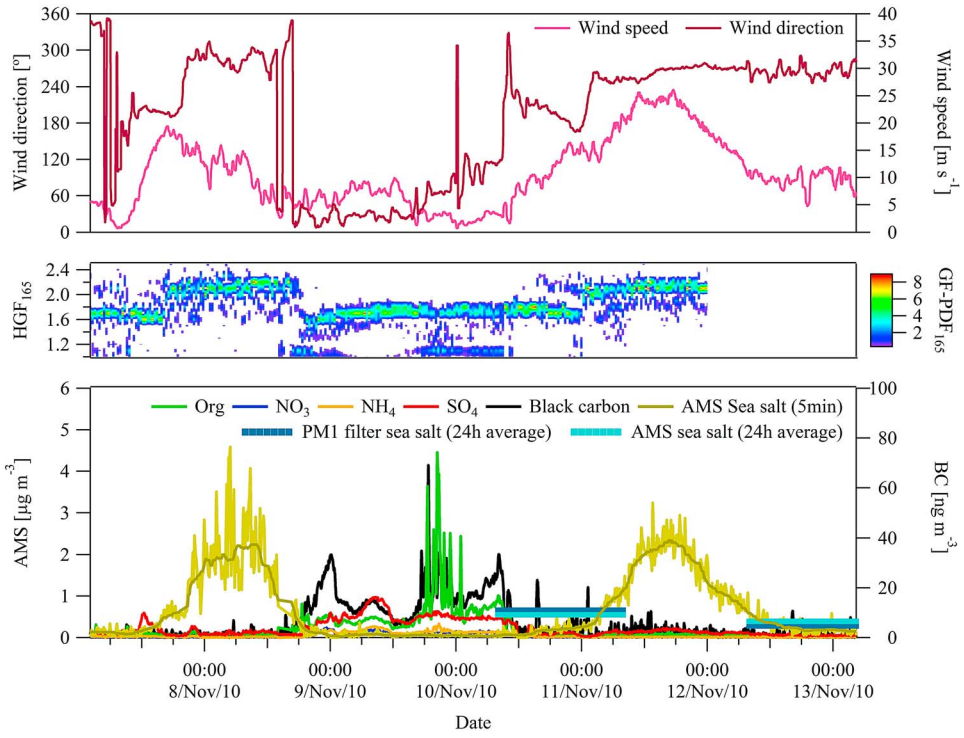

Figure 4. (top) Wind speed, wind direction observed for two sea salt plumes on 8th November 2009 and 11th November 2009. (middle) Hygroscopic growth factor for the corresponding period. (bottom) Five-minute and 24-h resolution sea salt mass derived from the HR-ToF-AMS and 24-h salt mass from the ion chromatography. Also shown are sulfate, nitrate, and organic masses from the AMS and black carbon mass from the MultiAngle Absorption Photometer.

speed (U_{10}) dependency, albeit with different exponents. For increasing wind speed, the power law exponent was higher ($U_{10}^{2.8}$) than the decreasing wind speed power law exponent ($U_{10}^{2.1}$). The net result indicates that mass concentrations measured during reducing wind speeds are significantly higher than those measured under increasing wind speeds.

[26] The difference between concentration-wind speed relationships for increasing and decreasing wind speed histories is consistent with the observed whitecap coverage dependency on wave history: whitecap coverage increases with wave age under the same wind speed conditions [*Callaghan et al.*, 2008; *Sugihara et al.*, 2007], suggesting that an increase in the sea salt production flux due to a higher whitecap coverage under decreasing wind fields compared to increasing wind fields.

[27] Submicron aerosol particles are expected to be uniformly mixed in the marine boundary layer [*Lewis and Schwartz*, 2004], thus an effective sea spray aerosol (SSA) production flux, F_{eff}, was estimated from the sea spray concentration (C) divided by a filling time (τ) and multiplied by the marine boundary layer height (H_{MBL}):

$$F_{eff} = \frac{C \times H_{MBL}}{\tau} \quad (1)$$

[28] The atmospheric boundary layer height, derived from the ground-based LIDAR measurements using the Temporal Height Tracking (THT) algorithm [*Haeffelin et al.*, 2012; *Milroy et al.*, 2012], was found to be within the range of 720–1290 m above the ground level over the plume duration period, while τ was assumed to be the filling time (approximately 1.5–2 days). This method is known as the Statistical Wet Deposition Method for estimation production flux and is critically discussed in *Lewis and Schwartz* [2004] who conclude that this approach cannot provide any information on the wind speed dependence of the sea salt production flux since the sea salt particles measured are likely to be produced far away under conditions different from local conditions at the time of measurement. However, we contend that in this particular case, we can apply the approach to determine a production flux for the following reasons: the deep low-pressure system associated with this plume event formed over the North East Atlantic approximately 1.5–2 days before arriving at Mace Head and we take τ, the filling time, not as the time since the last precipitation event as considered in *Lewis and Schwartz* [2004], but the time between the cyclone formation and subsequent arrival, in terms of connected flow, at Mace Head. Further, the local wind speed was representative of the upwind wind fields as obtained from NOAA Air Resources Laboratory for the 12:00 UTC 11 November 2010 (Figure 6).

[29] Although dry deposition is assumed to be negligible for the submicron particles [*Hoppel et al.*, 2002], it was taken into account and contributed 2–4% compared to the production flux. As mentioned, this period was practically cloud and precipitation free, which suggests that the wet-deposition and coalescence removal processes contributed to a similarly

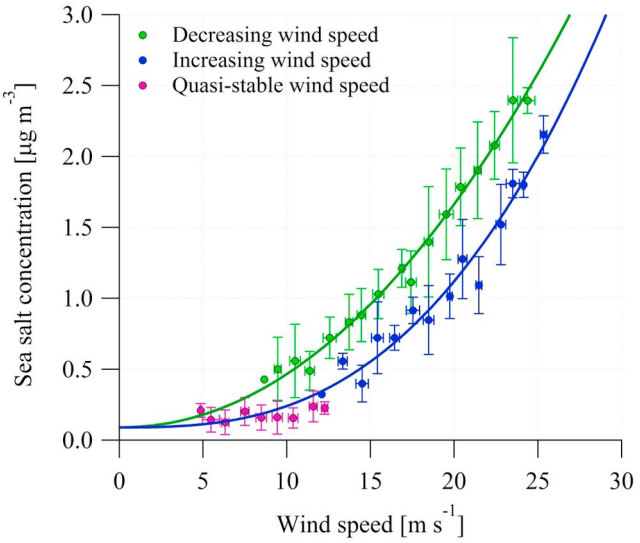

Figure 5. Sea salt wind speed–concentration relationships for increasing and decreasing wind speed history regimes: increasing is in dark blue; decreasing is in green. Purple represents quasi-stable wind speed conditions just after the decreasing wind speed regime (12:00 UTC 12th November–12:00 UTC 13th November 2010). Five-minute data points are binned to the wind speed intervals equal to 1 m s^{-1}.

negligible removal flux. The resulting production flux is represented in Figure 7.

[30] Without differentiating between increasing and decreasing wind speed regimes, and taking all the data into a single function relationship, the wind speed dependence converges to $F = 0.47 + 0.003U_{10}^{2.7}$, which is closely in line with the refitted sea spray production flux formulation from the *Geever et al.* [2005] ambient measurements [*O'Dowd et al.*, 2008]. Though, only the power exponent can be directly compared, as the coefficients would differ for a number flux (presented in *Geever et al.* [2005]) and a mass flux (presented in this study). Differentiating between increasing and decreasing wind speeds, the mass flux parameterizations are $F = 0.47 + 0.01U_{10}^{2.3}$ and $F = 0.47 + 0.0007U_{10}^{3.1}$, respectively. The intercept in the power function represents the starting aerosol flux at the onset of the whitecap, with the flux being 0 before the whitecap onset and making a step transition into minimum value after the onset. Assuming that the minimum wind speed needed for the onset of detectable whitecapping is approximately 3.7 m s^{-1} [*Callaghan et al.*, 2008], the minimum aerosol flux would be ~0.68 ng $m^{-2}s^{-1}$. Taking this into account, the flux equation should be expressed as follows:

$$F(U_{10}) = \begin{cases} 0 & \text{if } U_{10} < 3.7\,\text{m s}^{-1} \\ 0.47 + 0.003U_{10}^{2.7}, & \text{if } U_{10} \geq 3.7\,\text{m s}^{-1} \end{cases} \quad (2)$$

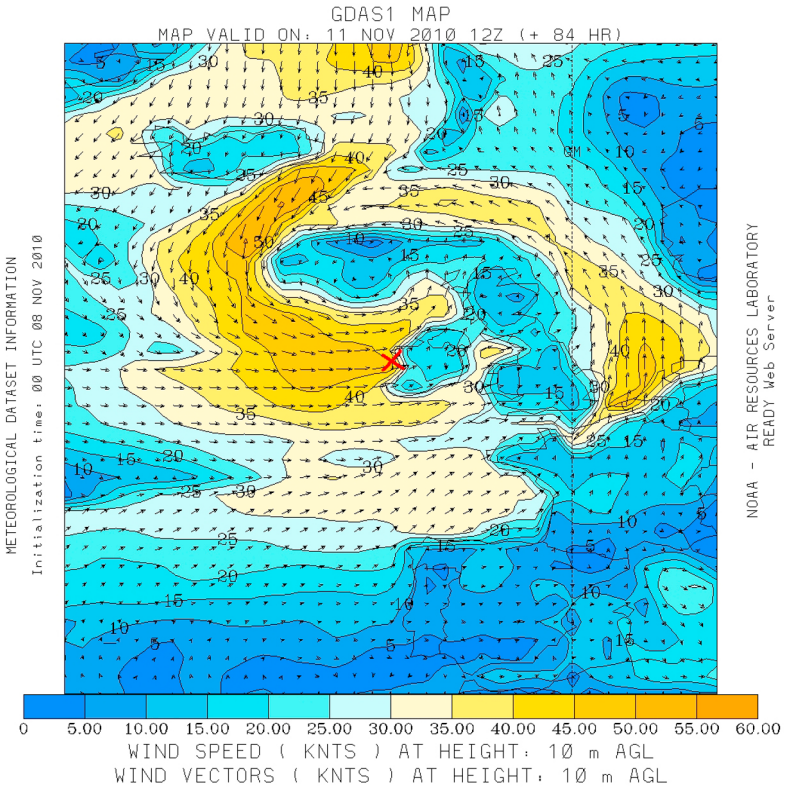

Figure 6. Wind speed field (in knots) for the 12:00 UTC 11 November 2010 obtained from the NOAA Air Resources Laboratory. Accordingly, the local wind speed measured at Mace Head was equal to 24.1 m s^{-1} (46.8 knots). It is in the rage of upwind wind speeds presented by NOAA (45–50 knots). Mace Head is marked in red.

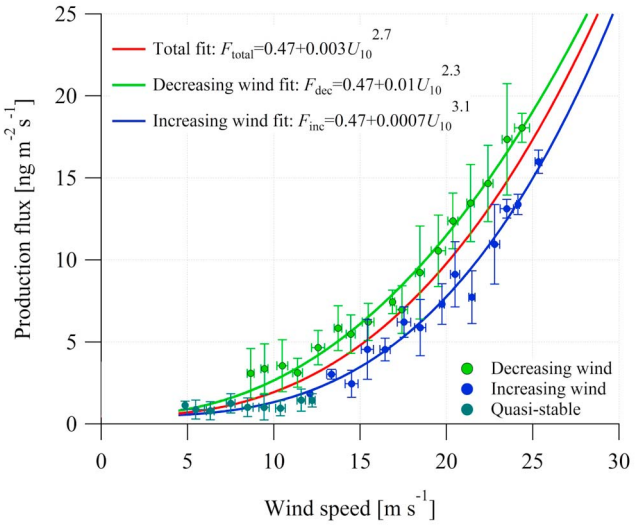

Figure 7. Sea spray production flux for increasing and decreasing wind speed history regimes. The intercept in the power function represents the starting aerosol flux at the onset of the whitecap, with the flux being 0 before the whitecap onset and making a step transition into minimum value after the onset.

[31] A more detailed comparison with existing source functions derived from the whitecap method is presented in Figure 8. Unfortunately, the original function from *Monahan et al.* [1986] is mainly valid for the particles larger than those measured by the HR-ToF-AMS, thus a comparison of the above scheme focuses on submicron flux parameterizations of *Gong* [2003] and *Mårtensson et al.* [2003], both of which are based on Monahan's whitecap–wind speed relationship. These particular parameterizations are extensively used in large-scale models. The corresponding number flux was simulated for a particle size range directly comparable to the AMS measurement size range (D_p = 0.03–0.58 μm or vacuum aerodynamic diameter, as measured in the HR-ToF-AMS, $D_{va} \cong$ 0.05–1 μm) and converted the integrated number flux over this size range into a corresponding mass flux as a function of wind speed. This comparison revealed a significantly more sensitive mass flux prediction as a function of wind speed for the *Gong* [2003] and *Mårtensson et al.* [2003] functions compared to the function presented from this study. This suggests that these source functions over-predict the sea salt flux as a function of wind speed - an apparent over-prediction supported the critical discussions in the recent *de Leeuw et al.* [2011] review paper, which suggests existing submicron number flux parameterizations appear to over-predict boundary layer number concentrations compared to what is actually measured. Even, the most-recent whitecap - aerosol productivity scheme, derived by *Fuentes et al.* [2010], also tends to over-predict boundary layer mass concentrations (Figure 8) relative to the current study. It should be noted that the current study is the only study of the four presented here which is based on field measurements.

[32] The mass flux calculations from the sea salt mass concentration involved the use of a filling time parameter τ, which determination from the air mass back trajectories could have had propagated some uncertainties into these calculations. Therefore, the grey area in Figure 8 represents the range of possible variations due to differences in τ. The largest reasonable filling time was assumed to be ~3 days (the typical lifetime of a submicron sea salt particle against precipitation scavenging [*Hoppel et al.*, 2002]) and the shortest was equal to 1 day. The filling time, which could have led to a fair agreement with the parameterization by *Gong* [2003], was estimated to be less than 10 h, which is regarded as unrealistically short, particularly given the lack of precipitation and cloud processes to contribute to removal mechanisms.

[33] There may be several reasons for the mass flux overestimation by the whitecap method: one relates is the whitecap area-to-wind speed parameterization; and another relates to the parameterization of aerosol number (or mass) productivity-to-whitecap area. The former parameterization has recently been improved on through analysis using digital image processing of sea-state photographs and removing the subjectivity in determining the intensity threshold that distinguishes whitecap from the surrounding water, along with the increased number of the averaging points [*de Leeuw et al.*, 2011]. Results of this new parameterization were presented in the study by *Callaghan et al.* [2008] and with a power law fitting of the same data set reported by *Goddijn-Murphy et al.* [2011].

[34] Taking into account an improved whitecap–wind speed relationship, we replaced the Monahan component with the *Callaghan et al.* [2008] whitecap scheme and

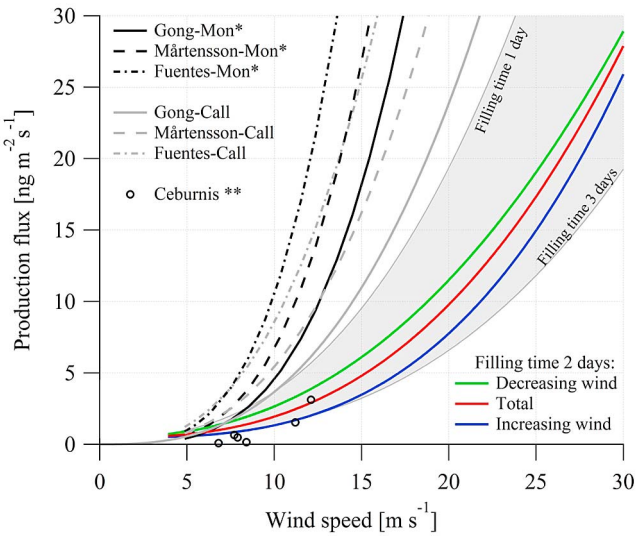

Figure 8. Production flux dependence on the wind speed. Color lines represent the flux derivations from the AMS sea salt measurements at different wind speed regimes. Grey area represents the measured flux uncertainty due to the different time of filling. Black lines illustrate the fluxes based on *Monahan and Muircheartaigh* [1980] whitecap–wind speed relationship and derived from *Gong* [2003], *Mårtensson et al.* [2003] and *Fuentes et al.* [2010] parameterizations. Grey lines represent the same parameterizations with the *Callaghan et al.* [2008] whitecap–wind speed relationship. One asterisk indicates that number flux presented in the original work was recalculated to the mass flux; two asterisks indicate sea salt fluxes calculated using data from *Ceburnis et al.* [2008].

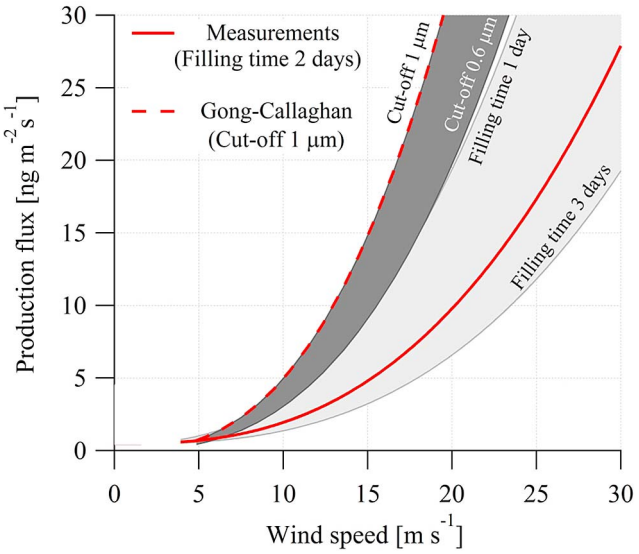

Figure 9. Production flux dependence on different vacuum aerodynamic size cut-offs assumed for the Gong-Callaghan parameterization. The dark grey area represents the uncertainty due to different cut-offs applied on the modeled mass flux distributions and the light grey area is the uncertainty of the production flux measured by the AMS (the same as in Figure 8). The most probable dependencies are presented in red.

found a reduced flux-to-wind speed dependency. The modified *Gong-Callaghan*, *Mårtensson-Callaghan and Fuentes-Callaghan* parameterizations, while leading to a much better agreement with our source function, still reside outside the range presented based on 1–2 days filling time (Figure 8).

[35] PM1 mass flux was also evaluated in the gradient study by *Ceburnis et al.* [2008], while they didn't provide the separate sea salt mass flux in the original paper, it is presented in Figure 8. The data points fell into grey area encompassing the range of uncertainty of the wet deposition statistical method, but the power law fitting is limited to a small number of data points and a restricted wind speed range of 12 m s^{-1}.

[36] In addition, the variation in the HR-ToF-AMS aerodynamic lens cut-off could have had an effect on the mass concentrations measured by the HR-ToF-AMS. Since the real lens transmission efficiency was not evaluated for this particular instrument, the sensitivity of the production flux to different assumed vacuum aerodynamic cut-offs applied for the modeled mass size distributions was tested. The typical HR-ToF-AMS aerodynamic lens cut-off of 1 μm (50% transmission efficiency for the particle vacuum aerodynamic diameter, D_{va}, of 1 μm or mobility diameter, D_m, of 0.58 μm) is applied to the Gong-Callaghan parameterization and presented as the upper limit of the modeled flux (Figure 9), whereas a cut-off of 0.6 μm (D_m of 0.35 μm) reflects the lower limit. The range in between these limits represents intermediate cut-off sizes. Reducing the cut-off size brings the modeled flux closer to the one measured by the HR-ToF-AMS, but only the extreme case of 0.6 μm cut-off partially overlaps with the uncertainty range of the HR-ToF-AMS measurements; however, it still remains far from the most probable measured flux suggested by this study (solid red curve in Figure 9). Considering that originally the Gong-Callaghan parameterization was the closest to the measurements in this study, the case of the Gong-Callaghan parameterization with 0.6 μm cut-off reflects the lowest possible limit for the modeled fluxes. All other parameterizations based on the *Monahan and Muircheartaigh* [1980] whitecap parameterization would, therefore, be significantly above the uncertainty range of the measurements.

[37] Ultimately, the source flux must be able to explain observed concentrations; however, using the *Gong* [2003], *Mårtensson et al.* [2003] or *Fuentes et al.* [2010] scheme leads to peak concentrations of 15.9 μg m^{-3}, 23.4 μg m^{-3} and 37 μg m^{-3} respectively for the maximum wind speed of 25 m s^{-1} (Table 1). These mass concentrations are simply too high for submicron sea salt mass concentrations at the reported wind speed, having never been observed. The overestimation is between a factor of 3–10 depending which source function is used. A good level of confidence in the sea salt mass concentrations derived from the AMS has been demonstrated both for the overall AMS-IC intercomparison (Figure 3) and for this particular plume (Figure 4), thus the remaining differences could be explained by drawbacks in either whitecap–wind speed relationship or aerosol productivity versus whitecap parameterization. Some improvement is seen in the use of a more recent whitecap–wind speed relationship (Figure 9 and Table 1), leaving more improvement required in the aerosol productivity versus whitecap parameterization. It should be noted that while there are some differences between the AMS-derived mass and filter-derived mass measurements, they are far from a factor of 3, and even farther from a factor of 10.

6. Conclusions

[38] A HR-ToF-AMS was tuned and calibrated to enable the quantification of submicron sea salt mass, which has not been achieved previously. The quantification was achieved by taking the $^{23}Na^{35}Cl^+$ ion as a surrogate for sea salt, corroborated by confirming a $^{37}Cl^+$ and $^{35}Cl^+$ isotope ratio of

Table 1. Mass Concentrations at Two Wind Speeds (10 and 25 m s^{-1}) Derived From Different Parameterizations[a]

	Mass Concentration (μg m^{-3})						
		Monahan's Whitecap–Wind Speed Relationship			Callaghan's Whitecap–Wind Speed Relationship		
Wind Speed	This Study (AMS)	Gong	Mårtensson et al.	Fuentes et al.	Gong	Mårtensson et al.	Fuentes et al.
10 m s^{-1}	0.3	0.8	1.1	1.7	0.6	0.9	1.3
25 m s^{-1}	2.6	15.9	23.4	37	6.6	9.8	15.4

[a]*Gong* [2003], *Mårtensson et al.* [2003], and *Fuentes et al.* [2010] aerosol production parameterizations applied with either *Monahan and Muircheartaigh* [1980] or *Callaghan et al.* [2008] whitecap–wind speed parameterization. Concentrations derived from the relationship presented in this study (equation (2)) are also shown. The boundary layer height of 1200 m and the filling time of 2 days were assumed for all calculations here.

3.13, and then identifying a calibration scaling factor through comparison with mono-disperse laboratory-generated synthetic sea salt aerosol. The HR-ToF-AMS was deployed to make ambient sea salt measurements in clean air at Mace Head and the results from two notable sea salt plumes are reported. Peak sea salt mass concentrations exceeding 4 μg m^{-3} were encountered although running mean concentrations were of the order of 2.4 μg m^{-3} (corresponding to a wind speed of $\sim$26 m s^{-1}). The mass concentration as a function of wind speed was found to follow a power law dependency on U_{10}; however, different exponents were observed for increasing and decreasing wind fields. Increasing winds led to a $U_{10}^{2.8}$ dependency while decreasing winds led to a $U_{10}^{2.1}$ relationship. One of the plumes was deemed suitable for extracting a mass flux source function. For the submicron aerosol mass flux–wind speed dependency, an exponent of 3.1 was found for increasing wind speeds and an exponent of 2.3 was found for decreasing wind speeds. Comparison to other source functions based on the Monahan wind speed–whitecap coverage suggested that existing source functions [e.g., *Gong*, 2003; *Mårtensson et al.*, 2003; *Fuentes et al.*, 2010] significantly over-estimate the source flux at all wind speeds below 25 m s^{-1}. Replacing the Monahan component of the source flux with the more recent *Callaghan et al.* [2008] whitecap–wind speed relationship brings the previous source functions closer to that presented in this study and based on the AMS measurements at Mace Head. However, we also conclude that the aerosol number, or mass, production parameterization as a function of whitecap coverage is also over-estimated.

[39] **Acknowledgments.** This work was supported by the Science Foundation Ireland (grant 08/RFP/GEO1233), HEA-PRTLI4 Environment and Climate: Impact and Responses program, European Commission IP EUCAARI, EPA-Ireland, and the European Space Agency (Support To Science Element: Oceanflux Sea Spray Aerosol). We would also like to thank Adrian Callaghan (NUI Galway and Scripps Institution of Oceanography, UCSD), Jose-Luis Jimenez (University of Colorado at Boulder) and Damien Martin (NUI Galway) for the valuable comments and discussions.

References

Alfarra, M. R., et al. (2004), Characterization of urban and rural organic particulate in the lower Fraser valley using two aerodyne aerosol mass spectrometers, *Atmos. Environ.*, *38*(34), 5745–5758, doi:10.1016/j.atmosenv.2004.01.054.

Allan, J. D., J. L. Jimenez, P. I. Williams, M. R. Alfarra, K. N. Bower, J. T. Jayne, H. Coe, and D. R. Worsnop (2003), Quantitative sampling using an Aerodyne aerosol mass spectrometer - 1. Techniques of data interpretation and error analysis, *J. Geophys. Res.*, *108*(D3), 4090, doi:10.1029/2002JD002358.

Allan, J. D., et al. (2004), Submicron aerosol composition at Trinidad Head, California, during ITCT 2K2: Its relationship with gas phase volatile organic carbon and assessment of instrument performance, *J. Geophys. Res.*, *109*, D23S24, doi:10.1029/2003JD004208.

Bahreini, R., E. J. Dunlea, B. M. Matthew, C. Simons, K. S. Docherty, P. F. DeCarlo, J. L. Jimenez, C. A. Brock, and A. M. Middlebrook (2008), Design and operation of a pressure-controlled inlet for airborne sampling with an aerodynamic aerosol lens, *Aerosol Sci. Technol.*, *42*(6), 465–471, doi:10.1080/02786820802178514.

Bahreini, R., et al. (2009), Organic aerosol formation in urban and industrial plumes near Houston and Dallas, Texas, *J. Geophys. Res.*, *114*, D00F16, doi:10.1029/2008JD011493.

Callaghan, A., G. de Leeuw, L. Cohen, and C. D. O'Dowd (2008), Relationship of oceanic whitecap coverage to wind speed and wind history, *Geophys. Res. Lett.*, *35*, L23609, doi:10.1029/2008GL036165.

Cavalli, F., et al. (2004), Advances in characterization of size-resolved organic matter in marine aerosol over the North Atlantic, *J. Geophys. Res.*, *109*, D24215, doi:10.1029/2004JD005137.

Ceburnis, D., C. D. O'Dowd, G. S. Jennings, M. C. Facchini, L. Emblico, S. Decesari, S. Fuzzi, and J. Sakalys (2008), Marine aerosol chemistry gradients: Elucidating primary and secondary processes and fluxes, *Geophys. Res. Lett.*, *35*, L07804, doi:10.1029/2008GL033462.

Chang, S. Y., and D. T. Allen (2006), Chlorine chemistry in urban atmospheres: Aerosol formation associated with anthropogenic chlorine emissions in southeast Texas, *Atmos. Environ.*, *40*, suppl. 2, 512–523, doi:10.1016/j.atmosenv.2006.04.070.

DeCarlo, P. F., et al. (2006), Field-deployable, high-resolution, time-of-flight aerosol mass spectrometer, *Anal. Chem.*, *78*(24), 8281–8289, doi:10.1021/ac061249n.

de Laeter, J. R., J. K. Bohlke, P. De Bievre, H. Hidaka, H. S. Peiser, K. J. R. Rosman, and P. D. P. Taylor (2003), Atomic weights of the elements: Review 2000 - (IUPAC technical report), *Pure Appl. Chem.*, *75*(6), 683–800, doi:10.1351/pac200375060683.

de Leeuw, G., E. L. Andreas, M. D. Anguelova, C. W. Fairall, E. R. Lewis, C. O'Dowd, M. Schulz, and S. E. Schwartz (2011), Production flux of sea spray aerosol, *Rev. Geophys.*, *49*, RG2001, doi:10.1029/2010RG000349.

Elbergali, A. K., and R. G. Brereton (1994), Influence of noise, peak position and spectral similarities on resolvability of diode-array high-performance liquid-chromatography by evolutionary factor-analysis, *Chemom. Intell. Lab. Syst.*, *23*(1), 97–106, doi:10.1016/0169-7439(93)E0068-F.

Facchini, M. C., et al. (2008), Important source of marine secondary organic aerosol from biogenic amines, *Environ. Sci. Technol.*, *42*(24), 9116–9121, doi:10.1021/es8018385.

Fuentes, E., H. Coe, D. Green, G. de Leeuw, and G. McFiggans (2010), On the impacts of phytoplankton-derived organic matter on the properties of the primary marine aerosol–Part 1: Source fluxes, *Atmos. Chem. Phys.*, *10*(19), 9295–9317, doi:10.5194/acp-10-9295-2010.

Gantt, B., N. Meskhidze, M. C. Facchini, M. Rinaldi, D. Ceburnis, and C. D. O'Dowd (2011), Wind speed dependent size-resolved parameterization for the organic mass fraction of sea spray aerosol, *Atmos. Chem. Phys.*, *11*(16), 8777–8790, doi:10.5194/acp-11-8777-2011.

Geever, M., C. D. O'Dowd, S. van Ekeren, R. Flanagan, E. D. Nilsson, G. de Leeuw, and U. Rannik (2005), Submicron sea spray fluxes, *Geophys. Res. Lett.*, *32*, L15810, doi:10.1029/2005GL023081.

Goddijn-Murphy, L., D. K. Woolf, and A. H. Callaghan (2011), Parameterizations and algorithms for oceanic whitecap coverage, *J. Phys. Oceanogr.*, *41*(4), 742–756, doi:10.1175/2010JPO4533.1.

Gong, S. L. (2003), A parameterization of sea-salt aerosol source function for sub- and super-micron particles, *Global Biogeochem. Cycles*, *17*(4), 1097, doi:10.1029/2003GB002079.

Haeffelin, M., et al. (2012), Evaluation of mixing-height retrievals from automatic profiling lidars and ceilometers in view of future integrated networks in Europe, *Boundary Layer Meteorol.*, *143*(1), 49–75, doi:10.1007/s10546-011-9643-z.

Hoppel, W. A., G. M. Frick, and J. W. Fitzgerald (2002), Surface source function for sea-salt aerosol and aerosol dry deposition to the ocean surface, *J. Geophys. Res.*, *107*(D19), 4382, doi:10.1029/2001JD002014.

Jimenez, J. L., et al. (2003), Ambient aerosol sampling using the Aerodyne Aerosol Mass Spectrometer, *J. Geophys. Res.*, *108*(D7), 8425, doi:10.1029/2001JD001213.

Kleefeld, C., C. D. O'Dowd, S. O'Reilly, S. G. Jennings, P. Aalto, E. Becker, G. Kunz, and G. de Leeuw (2002), Relative contribution of submicron and supermicron particles to aerosol light scattering in the marine boundary layer, *J. Geophys. Res.*, *107*(D19), 8103, doi:10.1029/2000JD000262.

Lewis, E. R., and S. E. Schwartz (2004), *>Sea Salt Aerosol Production: Mechanisms, Methods, Measurements and Models—A Critical Review*, *Geophys. Monogr. Ser.*, vol. 152, 413 pp., AGU, Washington, D. C., doi:10.1029/GM152.

Liu, P. S. K., R. Deng, K. A. Smith, L. R. Williams, J. T. Jayne, M. R. Canagaratna, K. Moore, T. B. Onasch, D. R. Worsnop, and T. Deshler (2007), Transmission efficiency of an aerodynamic focusing lens system: Comparison of model calculations and laboratory measurements for the Aerodyne Aerosol Mass Spectrometer, *Aerosol Sci. Technol.*, *41*(8), 721–733, doi:10.1080/02786820701422278.

Mårtensson, E. M., E. D. Nilsson, G. de Leeuw, L. H. Cohen, and H. C. Hansson (2003), Laboratory simulations and parameterization of the primary marine aerosol production, *J. Geophys. Res.*, *108*(D9), 4297, doi:10.1029/2002JD002263.

Matthew, B. M., A. M. Middlebrook, and T. B. Onasch (2008), Collection efficiencies in an Aerodyne Aerosol Mass Spectrometer as a function of particle phase for laboratory generated aerosols, *Aerosol Sci. Technol.*, *42*(11), 884–898, doi:10.1080/02786820802356797.

Middlebrook, A. M., R. Bahreini, J. L. Jimenez, and M. R. Canagaratna (2012), Evaluation of composition-dependent collection efficiencies for

the aerodyne aerosol mass spectrometer using field data, *Aerosol Sci. Technol.*, *46*, 258–271, doi:10.1080/02786826.2011.620041.

Milroy, C., et al. (2012), An assessment of pseudo-operational ground-based light detection and ranging sensors to determine the boundary-layer structure in the coastal atmosphere, *Adv. Meteorol.*, *18*, 929080, doi:10.1155/2012/929080.

Monahan, E. C., and I. O. Muircheartaigh (1980), Optimal power-law description of oceanic whitecap coverage dependence on wind-speed, *J. Phys. Oceanogr.*, *10*(12), 2094–2099, doi:10.1175/1520-0485(1980)010<2094:OPLDOO>2.0.CO;2.

Monahan, E. C., D. E. Spiel, and K. L. Davidson (1986), A model of marine aerosol generation via whitecaps and wave disruption, in *Oceanic Whitecaps and Their Role in Air-Sea Exchange Processes*, edited by E. C. Monahan and G. MacNiocaill, pp. 167–174, D. Reidel, Dordrecht, Netherlands.

Mulcahy, J. P., C. D. O'Dowd, S. G. Jennings, and D. Ceburnis (2008), Significant enhancement of aerosol optical depth in marine air under high wind conditions, *Geophys. Res. Lett.*, *35*, L16810, doi:10.1029/2008GL034303.

Nilsson, E., E. Swietlicki, S. Sjogren, J. Londahl, M. Nyman, and B. Svenningsson (2009), Development of an H-TDMA for long-term unattended measurement of the hygroscopic properties of atmospheric aerosol particles, *Atmos. Meas. Tech.*, *2*(1), 313–318, doi:10.5194/amt-2-313-2009.

O'Connor, T. C., S. G. Jennings, and C. D. O'Dowd (2008), Highlights of fifty years of atmospheric aerosol research at Mace Head, *Atmos. Res.*, *90*(2–4), 338–355, doi:10.1016/j.atmosres.2008.08.014.

O'Dowd, C. D., and M. H. Smith (1993), Physicochemical properties of aerosols over the Northeast Atlantic: Evidence for wind-speed-related submicron sea-salt aerosol production, *J. Geophys. Res.*, *98*(D1), 1137–1149, doi:10.1029/92JD02302.

O'Dowd, C. D., J. A. Lowe, M. H. Smith, and A. D. Kaye (1999), The relative importance of non-sea-salt sulphate and sea-salt aerosol to the marine cloud condensation nuclei population: An improved multi-component aerosol-cloud droplet parametrization, *Q. J. R. Meteorol. Soc.*, *125*(556), 1295–1313, doi:10.1002/qj.1999.49712555610.

O'Dowd, C. D., M. C. Facchini, F. Cavalli, D. Ceburnis, M. Mircea, S. Decesari, S. Fuzzi, Y. J. Yoon, and J. P. Putaud (2004), Biogenically driven organic contribution to marine aerosol, *Nature*, *431*(7009), 676–680, doi:10.1038/nature02959.

O'Dowd, C. D., B. Langmann, S. Varghese, C. Scannell, D. Ceburnis, and M. C. Facchini (2008), A combined organic-inorganic sea-spray source function, *Geophys. Res. Lett.*, *35*, L01801, doi:10.1029/2007GL030331.

Ovadnevaite, J., C. O'Dowd, M. Dall'Osto, D. Ceburnis, D. R. Worsnop, and H. Berresheim (2011), Detecting high contributions of primary organic matter to marine aerosol: A case study, *Geophys. Res. Lett.*, *38*, L02807, doi:10.1029/2010GL046083.

Rader, D. J., and P. H. McMurry (1986), Application of the tandem differential mobility analyzer to studies of droplet growth or evaporation, *J. Aerosol Sci.*, *17*(5), 771–787, doi:10.1016/0021-8502(86)90031-5.

Salcedo, D., et al. (2006), Characterization of ambient aerosols in Mexico City during the MCMA-2003 campaign with Aerosol Mass Spectrometry: Results from the CENICA Supersite, *Atmos. Chem. Phys.*, *6*, 925–946, doi:10.5194/acp-6-925-2006.

Salcedo, D., T. B. Onasch, A. C. Aiken, L. R. Williams, B. de Foy, M. J. Cubison, D. R. Worsnop, L. T. Molina, and J. L. Jimenez (2010), Determination of particulate lead using aerosol mass spectrometry: MILAGRO/MCMA-2006 observations, *Atmos. Chem. Phys.*, *10*(12), 5371–5389, doi:10.5194/acp-10-5371-2010.

Sugihara, Y., H. Tsumori, T. Ohga, H. Yoshioka, and S. Serizawa (2007), Variation of whitecap coverage with wave-field conditions, *J. Mar. Syst.*, *66*(1–4), 47–60, doi:10.1016/j.jmarsys.2006.01.014.

Sullivan, A. P., R. J. Weber, A. L. Clements, J. R. Turner, M. S. Bae, and J. J. Schauer (2004), A method for on-line measurement of water-soluble organic carbon in ambient aerosol particles: Results from an urban site, *Geophys. Res. Lett.*, *31*, L13105, doi:10.1029/2004GL019681.

Vignati, E., M. C. Facchini, M. Rinaldi, C. Scannell, D. Ceburnis, J. Sciare, M. Kanakidou, S. Myriokefalitakis, F. Dentener, and C. D. O'Dowd (2010), Global scale emission and distribution of sea-spray aerosol: Sea-salt and organic enrichment, *Atmos. Environ.*, *44*(5), 670–677, doi:10.1016/j.atmosenv.2009.11.013.

Weber, R., et al. (2003), Intercomparison of near real time monitors of PM2.5 nitrate and sulfate at the U.S. Environmental Protection Agency Atlanta Supersite, *J. Geophys. Res.*, *108*(D7), 8421, doi:10.1029/2001JD001220.

Zhang, X., K. A. Smith, D. R. Worsnop, J. L. Jimenez, J. T. Jayne, C. E. Kolb, J. Morris, and P. Davidovits (2004), Numerical characterization of particle beam collimation: Part II integrated aerodynamic-lens–nozzle system, *Aerosol Sci. Technol.*, *38*(6), 619–638, doi:10.1080/02786820490479833.